Biointerface Research in Applied Chemistry
Open-Access Journal (ISSN: 2069-5837)

Article
Volume 14, Issue 5, 2024, 125
https://doi.org/10.33263/BRIAC145.125

Electron Trapping Ionic Battery Using Graphene and Niobium Coated Electrodes: Simulations and Real Concept

Diogo José Horst [1,*], Charles Adriano Duvoisin [1], Edson Luiz Valmorbida [2,*], Diane Dias [3]

[1] Chemical Engineering Department, Federal University of São Paulo (UNIFESP), Diadema – SP, 09913-030, Brazil
[2] Department of Mathematics, Federal University of Technology – Paraná (UTFPR), Londrina – PR, 06036-370, Brazil
[3] Analytical Electro-Spectrum Department, Federal University of Rio Grande (FURG), Rio Grande – RS, 96203-900, Brazil
* Correspondence: diogohorst@gmail.com;

Scopus Author ID 55823621400
Received: 9.04.2024; Accepted: 12.05.2024; Published: 22.07.2024

Abstract: Niobium/graphene-based materials have strong thermodynamic and electrical stability among the present options, ensuring good safety performance for batteries and capacitors. This work demonstrates a prototype ionic battery based on electron trapping by combining computational and experimental approaches. Using EDOs: ode23t technique, a mathematical model was constructed to control the battery's charge/discharge module. We study the electrical and thermal performance as well as the synergic effect of the CVD-coated graphene/niobium electrodes. Electrochemical, XRD, SEM, TEM, and EDS measurements were used to characterize the materials. According to the data, the load cell can charge 2.1 Amperes per minute and discharge completely for a certain amount of time. The electrolyte temperature for both acid and base media is 22°C, and the 140 kV electric field does not cause overheating in the system. Both the graphene oxide and niobium pentoxide-covered electrodes have anode potentials between 1.25 and 1.5, which are comparable to the potentials of platinum and gold.

Keywords: graphene; niobium; oxides; electrons trap; ionic battery; electrodes; simulations; concept.

1. Introduction

Rechargeable batteries and supercapacitors are two examples of energy storage technologies that have recently contributed significantly to the quickly changing technological landscape by lowering reliance on fossil fuels. These systems are crucial because they allow for dependable and effective energy storage for a range of uses [1-4].

Energy storage systems must be able to charge quickly nowadays in order to be used in electrical power grids and electric automobiles. High-rate electrode materials, which have been produced by various techniques, including nanosizing, porous structures, carbon coatings, and conductive materials-based hierarchical structures, enable the quick charging performance of batteries [5-8].

Higher current densities can be achieved by improving the electrodes' electrical conductivity through the use of carbon coatings and conductive materials like graphene or Mxene-based hierarchical structures. Carbonaceous materials were employed as electrode materials because of their great electrical conductivity, chemical stability, mechanical toughness, high working potential, and corrosion resistance in acidic solutions [9-13].

Versatile electrode materials have been employed to enhance storage efficiency; materials based on niobium (Nb) have garnered significant interest because of their exceptional performance, distinct crystal structures, and unique characteristics, such as corrosion resistance in a strong acid solution [14-17].

Model simulation is a crucial technique for the safety design of battery systems and a useful way to investigate the features of thermal runaway propagation and electrical behavior [18,19].

Experimental analysis is very realistic, but it still costs money and takes a lot of time. Battery management design is efficiently guided, and simulation calculations greatly reduce research expenses. However, maintaining simulation realism remains a significant difficulty [20,21].

In this respect, this work examines the synergy between graphene and niobium-coated electrodes to enhance a battery's charging and discharging capacity based on electron trapping. Both the actual battery concept and the programming for the charge management module are shown. The presentation includes the characterization, synthesis, performance validation, and processing of the materials, in addition to a basic grasp of the functional mechanisms.

2. Materials and Methods

This section presents the methodological procedures used in the development of this study.

2.1. Circuit design, simulation development, and prototype built.

The electric circuit was designed using Multisim software (Figure 1). The electrode cell works with a constant electric field of 140 kV. The mathematical models used to simulate applied loads' thermal and electrical behavior and manage battery charging and discharging were developed using the Matlab EDOs: ode23t methodology (Figure 2). Figure 3 shows the PWM frequency x voltage. Figure 4 shows the internal thermal behavior of the system. The full-scale prototype is shown in Figure 5. Figure 6 shows the relationship between charging and discharging.

2.2. Synthesis and coating of electrodes with graphene and niobium.

All chemicals used are commercially sourced products of analytical grade without any additional purification. $Nb_3O_7(OH)$ was synthesized by a hydrothermal method. Niobium chloride ($NbCl_5$) was added to a 5 M hydrochloric acid (HCl) solution under stirring for 30 min, and then the obtained solution was transferred to a Teflon-lined stainless steel autoclave. The hydrothermal reaction was maintained at a constant temperature of 210°C for 24 hours.

The autoclave was cooled naturally to room temperature, and the $Nb_3O_7(OH)$ nanorods were collected by centrifugation and washed with deionized water until the pH value of the colloidal solution was neutral. The $Nb_3O_7(OH)$ crystalline powder was dried in an oven at 50°C for 24 h. Graphene oxide was synthesized using the modified Hummers method. This method dispersed 0.1 g of GO in 100 mL of ethanol, and the pH value was adjusted to 4 by adding 5 M HCl. Subsequently, it was mixed with 0.05 g of $Nb_3O_7(OH)$ powder to obtain a weight ratio of 2:1 between $Nb_3O_7(OH)$ and GO. The solution was then refluxed at a constant temperature at the boiling point of ethanol under vigorous stirring for 10 hours. Then, the colloidal solution was immediately transferred to the autoclave. The hydrothermal temperature was set at 150°C

for 3 h, and the collected catalyst was represented as $Nb_3O_7(OH)$/rGO. The $Nb_3O_7(OH)$/rGO was then annealed in a nitrogen atmosphere at 450°C, 850°C, and 1050°C. After this step, the samples were characterized by different techniques, which identified and represented them as Nb_2O_5/rGO, $Nb_{12}O_{29}$/rGO, and NbO_2/NbC/rGO at 450°C, 850°C, and 1050°C, respectively.

Graphene and niobium oxide nanoparticles were deposited on copper electrodes in rods and plates using a CVD process for the coatings. The depositions were carried out on an Annealsys RT-CVD with the initial conditions of previous investigations, with adjustments for a copper electrode as substrate. High-purity nitrogen, hydrogen, and methane gases were added to the growth process at 10-2 Torr pressure. The growth process was carried out at 950°C, and an atmosphere of methane (10 sccm) mixed with 1000 sccm of nitrogen and hydrogen was required for film growth for 15 minutes. After this time, the cooling step was carried out from 950°C to room temperature—figure 7 shows coated rod-shaped copper electrodes and coated battery plates (anode and cathode).

2.3. Morphology and particle size distribution.

The images of the superficial morphology of samples (Figure 8) were obtained using scanning electron microscopy SEM (FESEM, JSM 6500F, JEOL). Transmission electron microscopy (Figure 9) (FETEM, JEOL 2100), equipped with energy-dispersive X-ray spectroscopy EDXA (Table 1 and Table 2). The particle size distribution of Nb2O5 (A) and GO (B) nanoparticles is shown in Figure 10.

2.4. X-ray diffraction.

X-ray photoelectron spectroscopy (VG Scientific ESCALAB 250) was used to analyze the chemical components and oxidation states of the elements present in the samples. The crystalline structures were investigated by a Bruker D2-phaser using X-ray diffraction (XRD) technology with a Cu Kα light source, as shown in Figure 11.

2.5. Electrochemical experiments.

The cyclic voltammetry was made using a PGSTAT128N (EcoChemie, Utrecht, Netherlands) with a three-electrode system composed of an Ag|AgCl|KCl (saturated) reference electrode, a platinum wire as the auxiliary electrode and a modified copper electrode as the working electrode. The copper electrode was modified by chemical vapor deposition with niobium and graphene oxides (Figure 12).

3. Results and Discussion

The electrical diagram created with the Multisim program is displayed in Figure 1. The electrode cell operates with a continuous electric field of 140 kV, whereas the circuit operates at 24V c/c. This permits the load cell to experience the effects of the electric field, enabling quick and effective controlled charging and discharging.

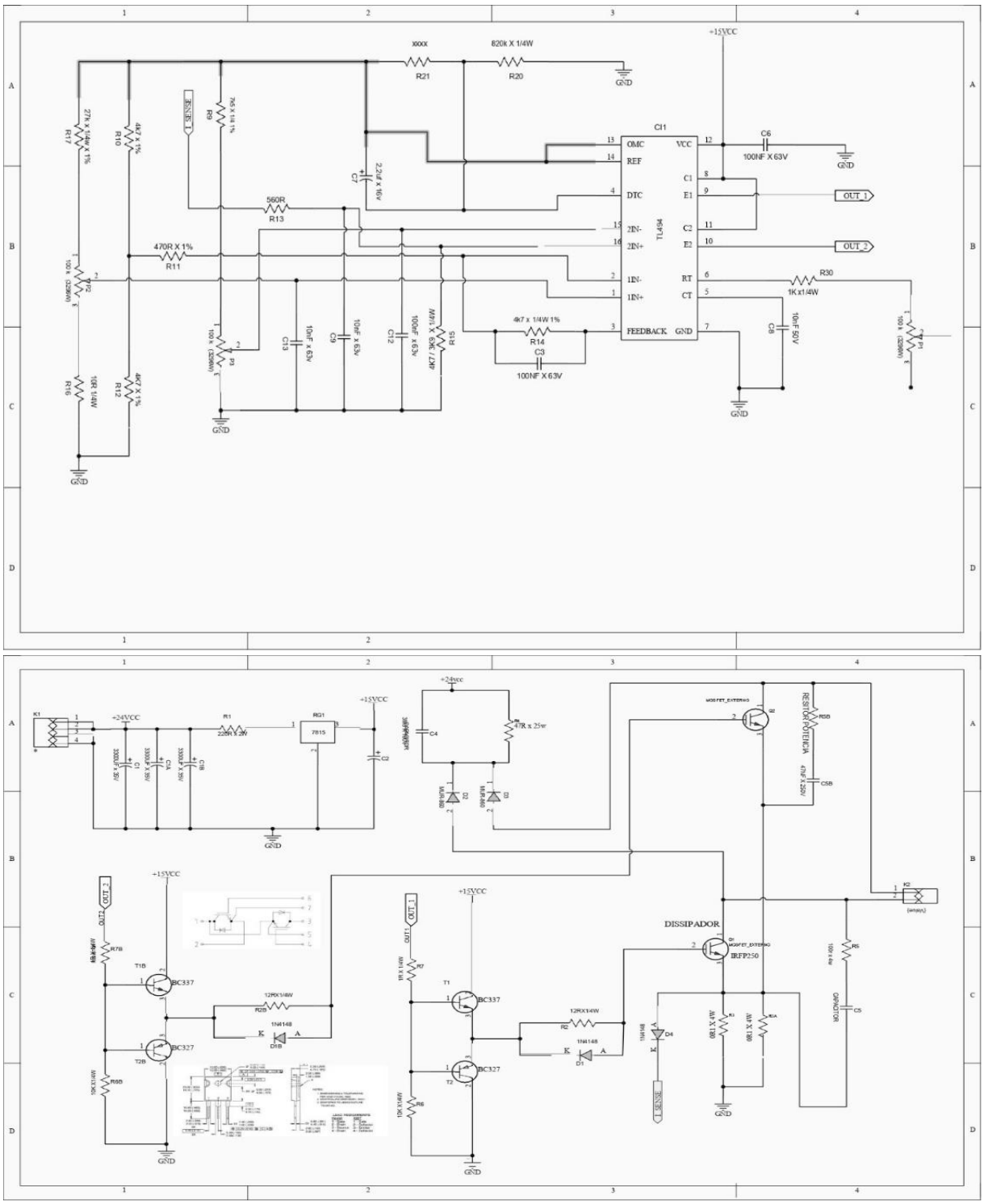

Figure 1. Electrical schematic diagram of the ionic battery based on electrons trap.

The simulation diagram programmed using Matlab for battery energy and temperature management is shown in Figure 2.

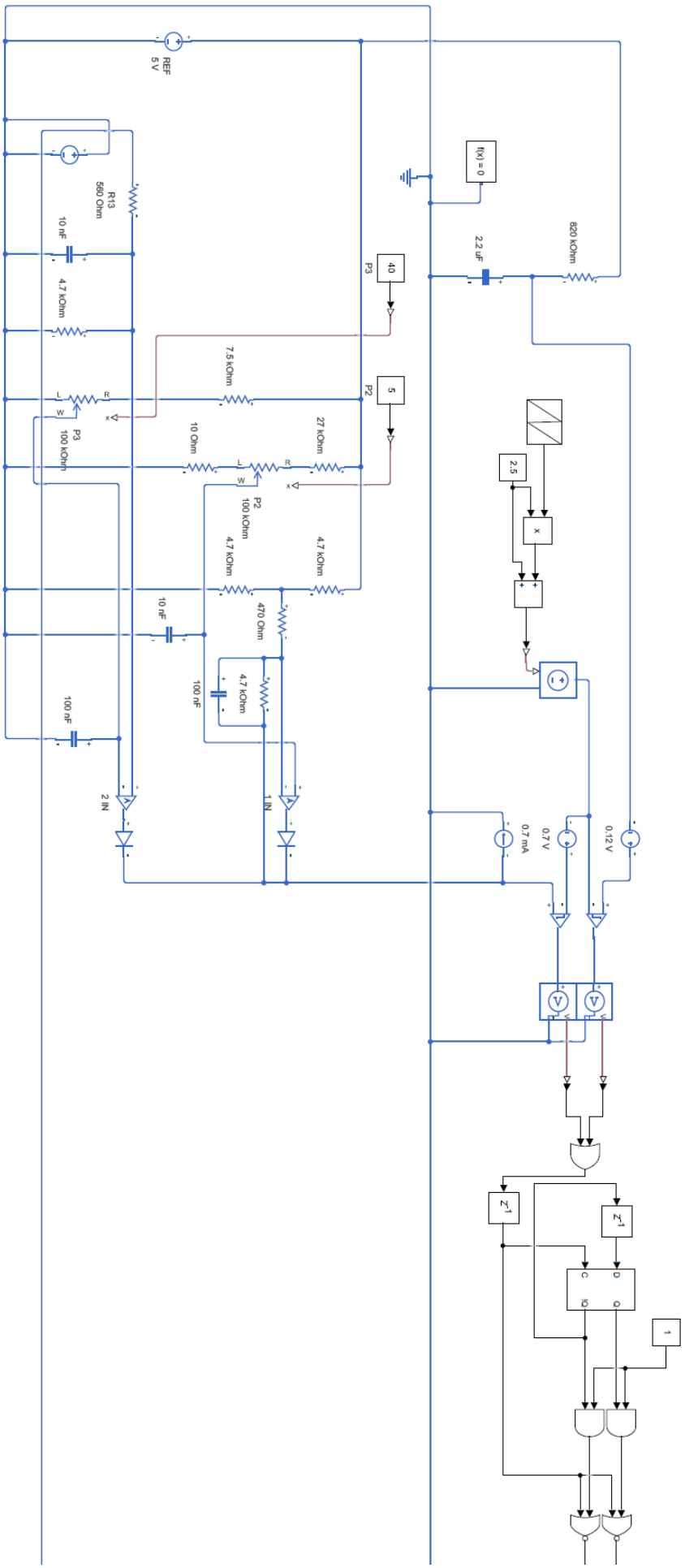
REF
5 V
R13
560 Ohm
10 nF
4.7 kOhm
P3
100 kOhm
7.5 kOhm
10 Ohm
27 kOhm
P2
100 kOhm
4.7 kOhm
4.7 kOhm
10 nF
470 Ohm
100 nF
4.7 kOhm
100 nF
2 IN
1 IN
f(x) = 0
2.2 uF
820 kOhm
40
P3
5
P2
2.5
x
0.7 mA
0.7 V
0.12 V
Z-1
Z-1
C
D
Q
1

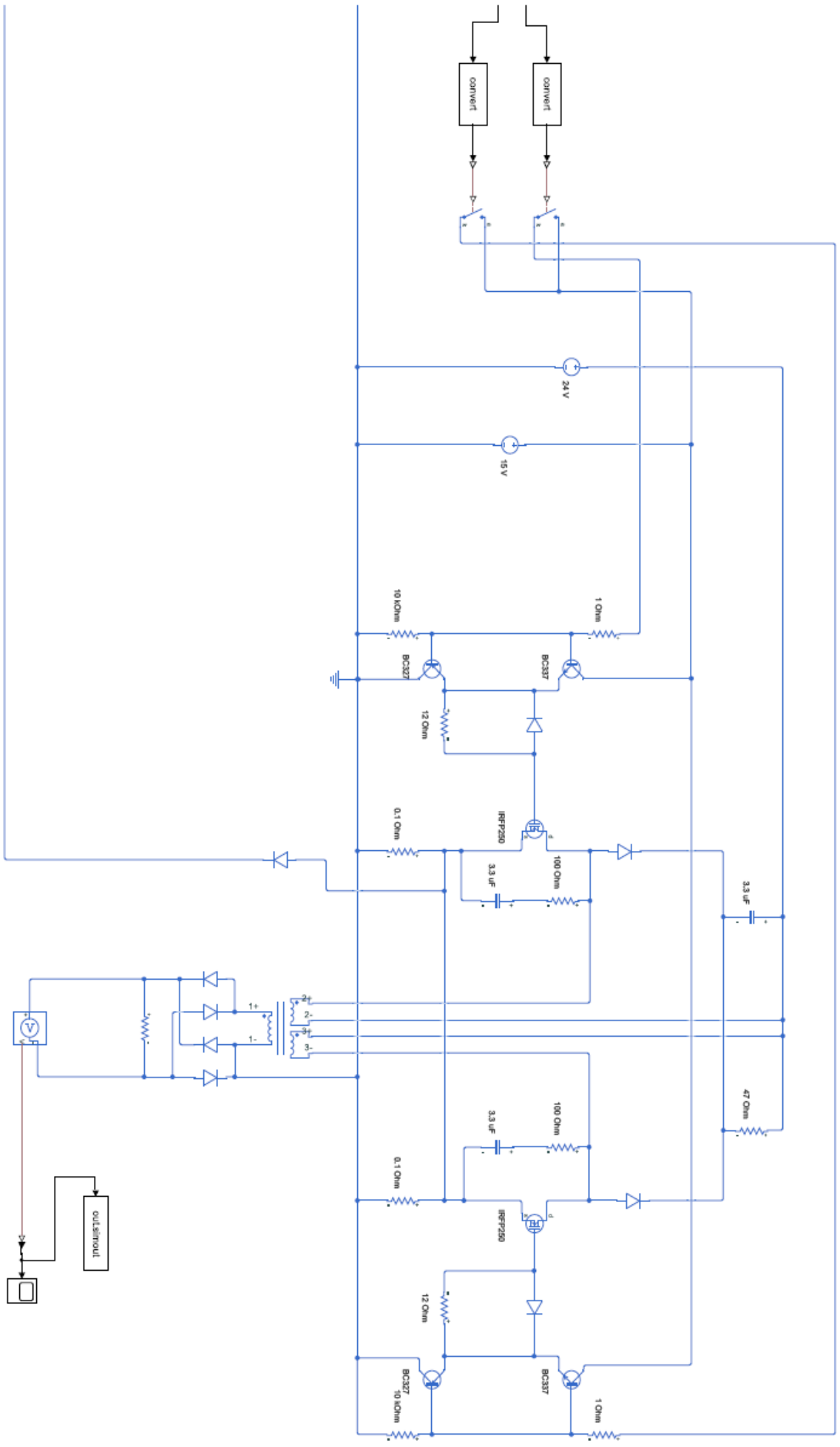

Figure 2. Battery management design developed using the Simscape battery application and Matlab.

Figure 3, exposed below, shows the voltage x frequency of pulse width modulation (PWM).

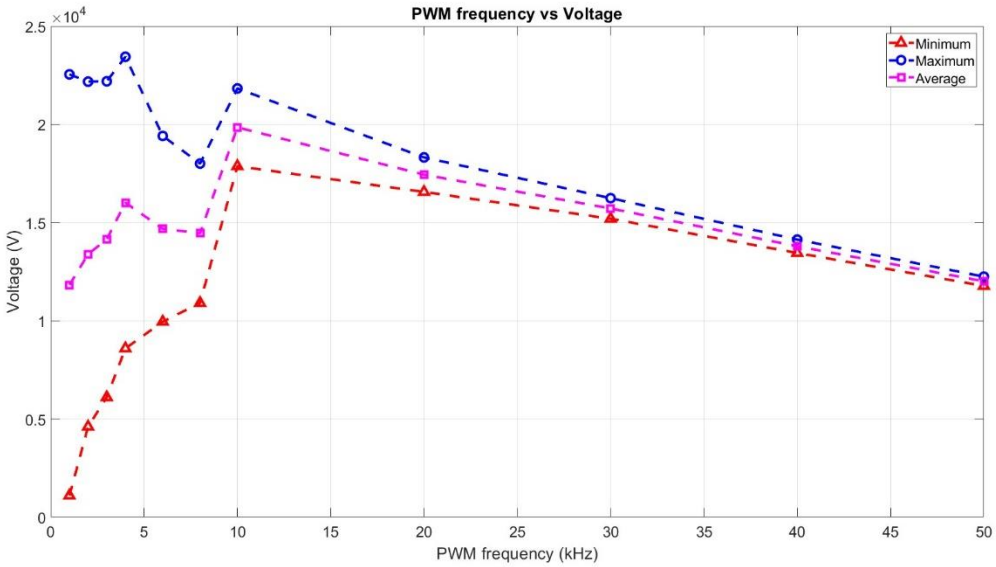

Figure 3. PWM frequency x voltage simulation.

The simulation of the high-voltage generator circuit is divided into two parts: the PWM controller and the power circuit.

The PWM controller simulation is basically composed of a sawtooth wave generator connected to the inverting input of two comparator amplifiers, whose outputs pass through a digital logic that generates two complementary PWM signals. A passive circuit with a potentiometer for adjusting the PWM pulse width is mounted at the non-inverting input of one of the comparators. A passive circuit for feedback to the power circuit is mounted at the non-inverting input of the other comparator, with a potentiometer for adjusting feedback sensitivity.

The power circuit is made up of two transistorized power amplifiers, which are driven by complementary signals from the PWM controller, and these amplifiers feed a high-voltage transformer. Finally, the power circuit provides voltage feedback from the amplifiers to the PWM controller.

The system's thermal behavior is shown in Figure 4; the load cell's internal temperature stays between 20 and 22 °C during testing, indicating that the 140 kV electric field does not cause excessive heating.

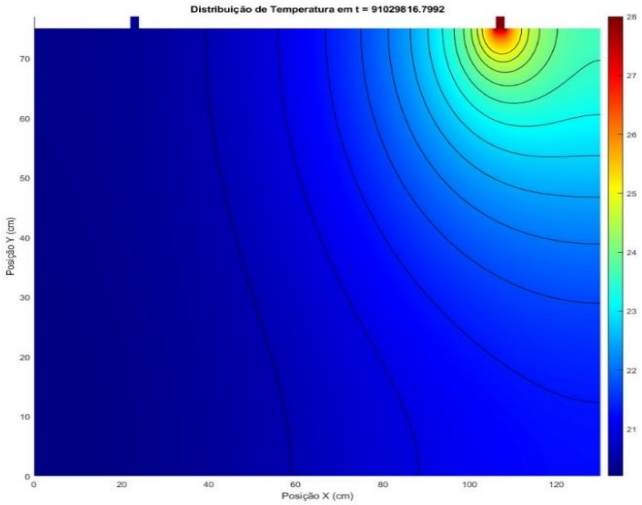

Figure 4. Thermal behavior of electrodes in operation.

The full-scale ionic battery prototype is shown in Figure 5.

Figure 5. A full-scale prototype of the ionic battery based on electron trap. Caption: **1)** circuit breaker; **2)** control board; **3)** power supply; **4)** insulated-gate bipolar transistor; **5)** cooler; **6)** transformer driver; **7)** high voltage power transformer (i); **8)** high voltage power transformer (ii); **9)** rectifier diodes; **10)** battery cell; **11)** positive and negative electrodes.

The relationship between charging and discharging using niobium pentoxide-coated electrodes is shown in Figure 6.

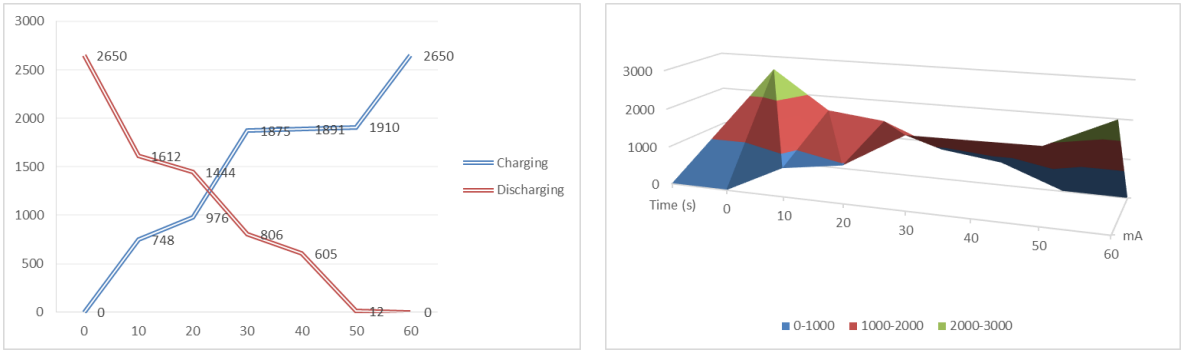

Figure 6. Charging/discharging in 60 s for Nb_2O_5-covered electrodes.

The relationship between charging and discharging using graphene-coated electrodes is shown in Figure 7.

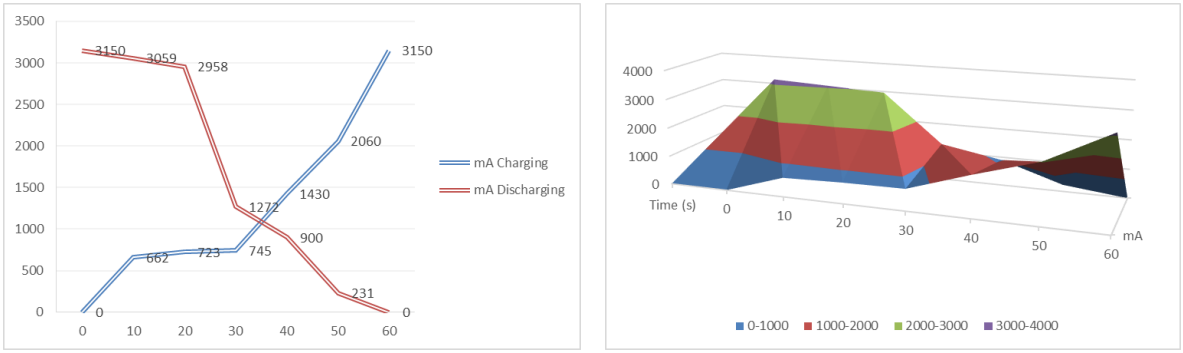

Figure 7. Charging/discharging in 60 s for graphene-coated electrodes.

The relationship between charging and discharging using copper electrodes without coating is shown in Figure 8.

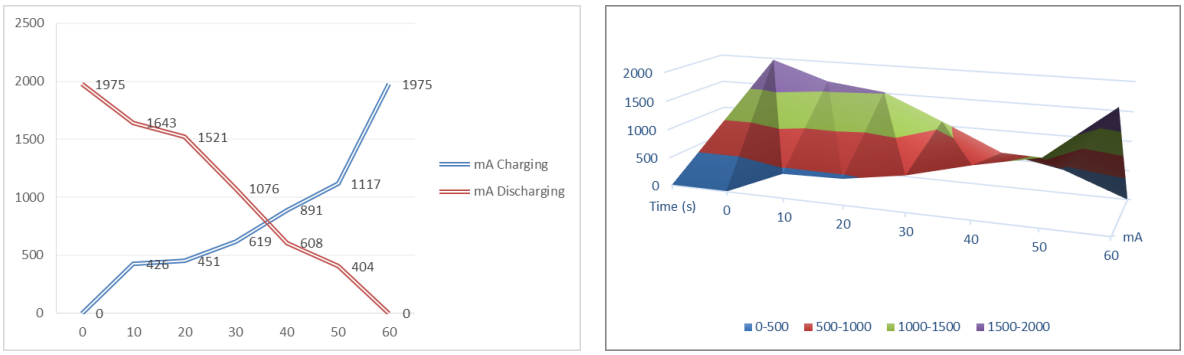

Figure 8. Charging/discharging in 60 s for copper electrodes without coating.

When assembling the battery concept, we tested only 1 load cell; in future studies, we intend to demonstrate the charging of several cells in series as well as their automation control.

Figure 9, exposed below, shows the rod and plate-shaped coated electrodes.

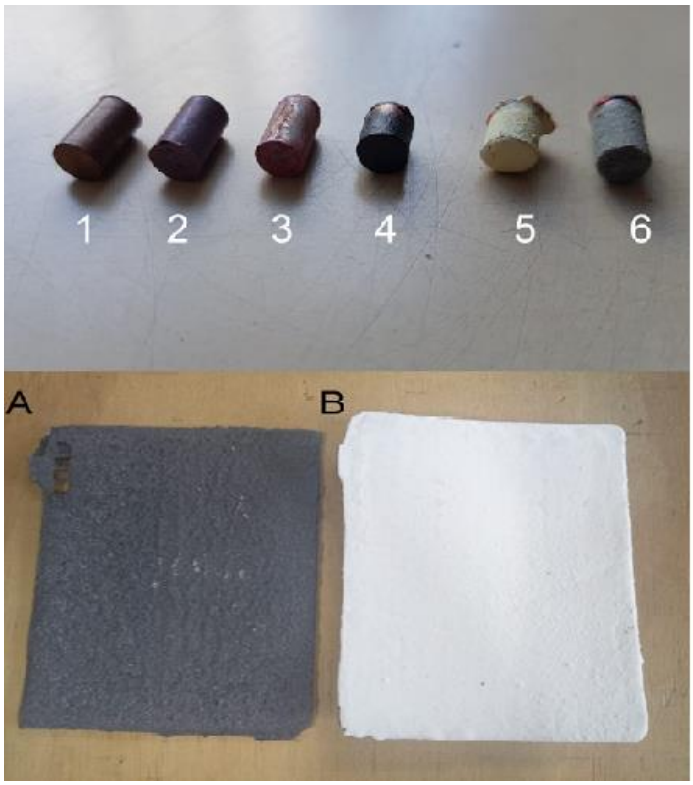

Figure 9. Rod-shaped and plate battery-coated electrodes. Caption: **1)** uncoated; **2)** coated with GO CVD; **3)** coated with Nb_2O_5 CVD; **4)** coated with graphene; **5)** coated with niobium; **6)** mixed GO/Nb_2O_5; **A)** anode coated with graphene oxide; **B)** cathode coated with niobium pentoxide.

Figure 10 shows the surface morphology of the particles using SEM.

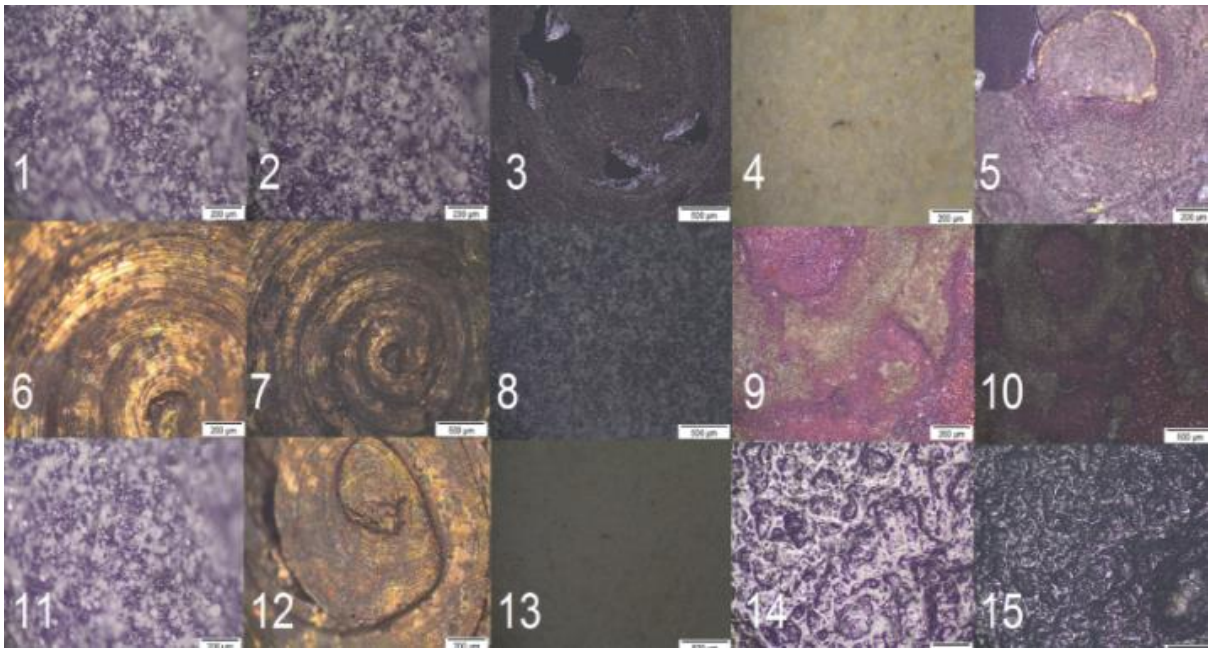

Figure 10. Morphology of samples by SEM. Caption: samples 1 and 2 growth of niobium nanograins, 4 and 5 growth of graphene, 3 and 6 Nb_2O_5 + GO mixed.

Figure 11 shows the surface morphology of the particles using TEM.

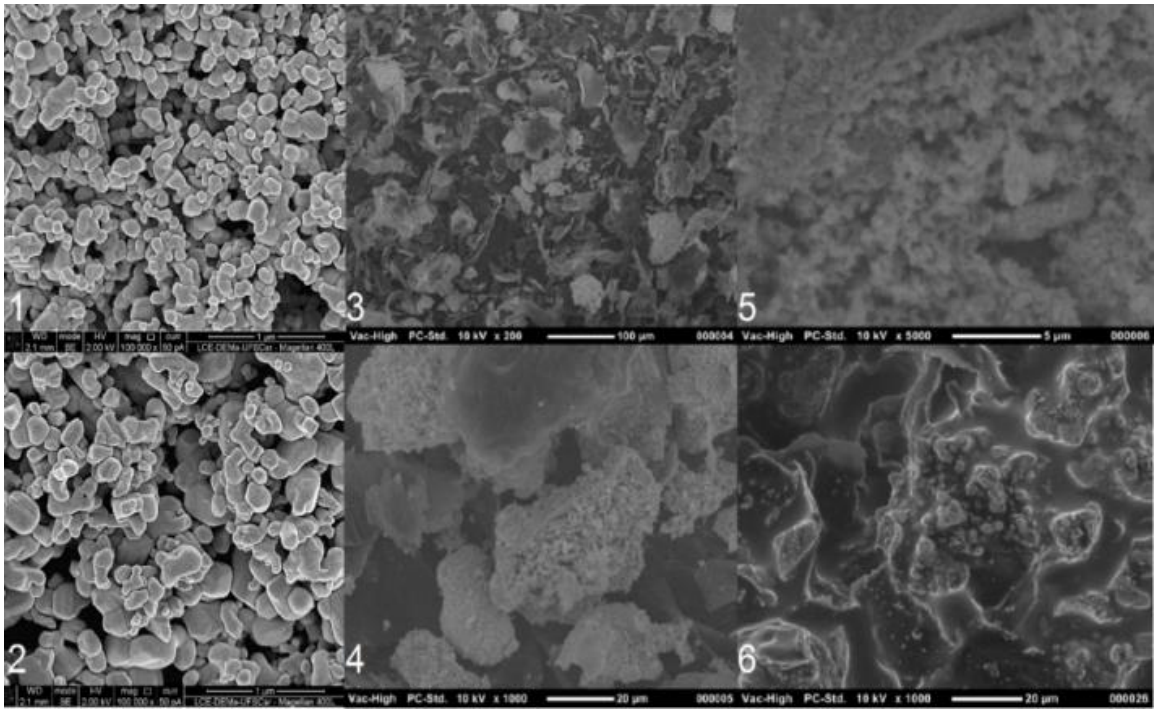

Figure 11. Morphology of samples by TEM. Caption: 1, 2, 4, 5, 8, 9, 10, 11, and 13 coating of the rod-shaped electrode with Nb_2O_5 nanoparticles, 3, 6, 7, 12 coating of the rod-shaped electrode with GO nanoparticles, 14 and 15 mixed coating of Nb_2O_5 + GO electrode on plate by CVD.

Tables 1 and 2 show the EDS chemical analysis of the obtained Nb_2O_5 and GO nanoparticles.

Table 1. Chemical composition of Nb_2O_5.

Component	Composition
Nb_2O_5 %	99,6
S (ppm)	1865
Ta (ppm)	1024

Component	Composition
K (ppm)	715
Fe (ppm)	181
Na (ppm)	136
Si (ppm)	182
P (ppm)	85
LOI %	0,7

Table 2. Chemical composition of GO.

Component	Composition
GO %	99,7
C (ppm)	6702
O (ppm)	3185
S (ppm)	094
Cu (ppm)	017
LOI %	0,02

Figure 12 shows the particle size distribution, and Figure 13 presents the DRX analysis.

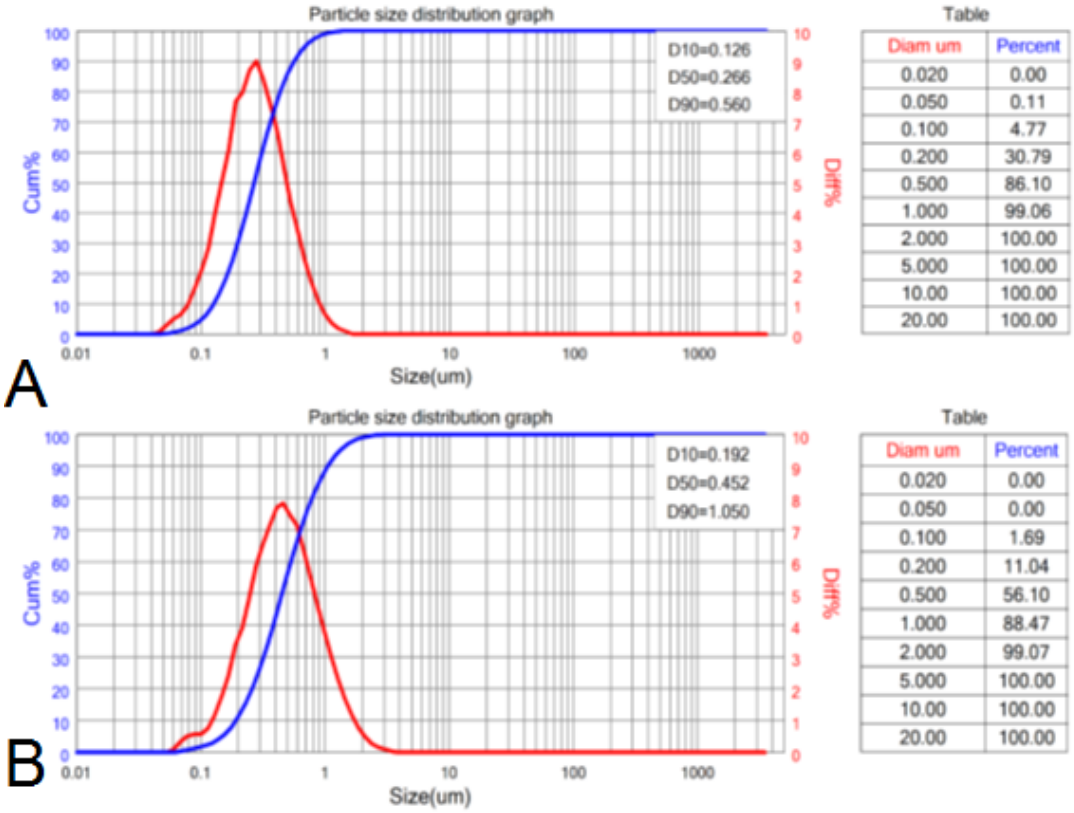

Figure 12. Particle size distribution of **(A)** Nb_2O_5; **(B)** GO nanoparticles.

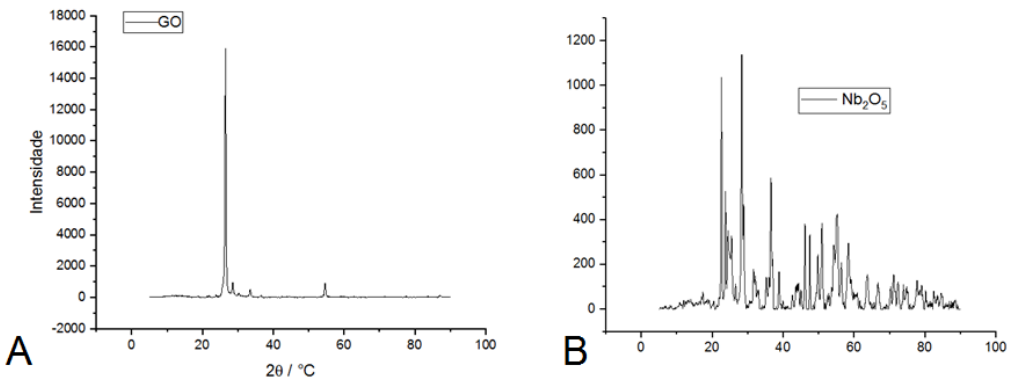

Figure 13. Diffractogram of samples. Caption: **A)** graphene oxide crystalline structure; **B)** niobium pentoxide orthorhombic crystal structure.

Figure 14 shows the electrochemical measurements.

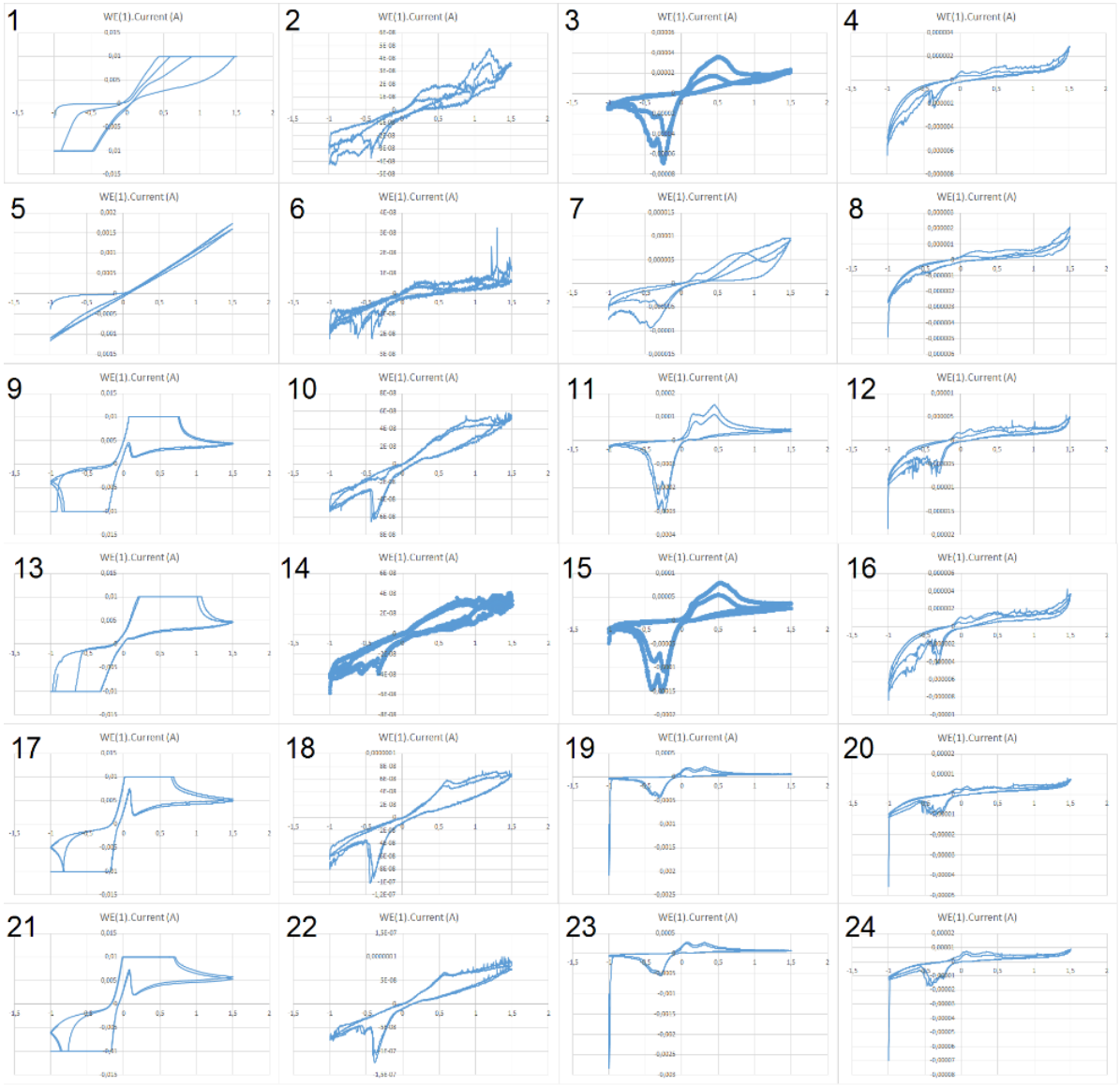

Figure 14. Electrodes cyclic voltammogram. Caption: **1)** uncoated sample; **2)** Nb_2O_5 coating; **3)** Nb_2O5 + GO mixed coating; **4)** graphene GO coating. Graphene and niobium oxides have anodic potentials between 1.25 and 1.5, comparable to platinum and gold's potentials. For both basic and acidic media, the limiting cathodic potential of both materials is -1.0.

4. Conclusions

Among the current alternatives, materials based on niobium and graphene offer great thermodynamic and electrical stability, guaranteeing good safety performance for batteries and capacitors. This study combines computational and experimental methods to establish a prototype ionic battery based on electron trapping. A mathematical model was created to regulate the battery's charge/discharge module using the EDOs: ode23t approach. We investigate the CVD-coated graphene/niobium electrodes' electrical, thermal, and synergic properties. The materials were characterized by XRD, SEM, TEM, electrochemical, and EDS measurements. The data indicates the load cell has a 2.1 Amperes per minute charging capacity and a full discharge time. Both acid and base media have an electrolyte temperature of 22°C, and the 140 kV electric field prevents the system from overheating. The anode potentials of the electrodes coated with graphene oxide and niobium pentoxide range from 1.25 to 1.5, similar to platinum and gold's potentials.

Funding

This work was supported by the Innovative Research in Small Businesses Program - PIPE, procedure number [2022/13473-3], FAPESP, Brazil.

Acknowledgments

The authors are thankful toThe Federal University of São Paulo and the Federal University of Rio Grande, which offered instructors and technicians for the laboratory essays.

Conflicts of Interest

The authors declare no conflict of interest.

References

1. Aghamohammadi, H.; Eslami-Farsani, R.; Iranipour Oskouei, H. Electrochemical performance of $TiNb_2O_7$/graphene/CNTs hybrid nanocomposites as anode materials for Li-ion batteries. *Diam. Relat. Mater.* **2024**, *141*, 110654, https://doi.org/10.1016/j.diamond.2023.110654.
2. Amir, M.; Deshmukh, R.G.; Khalid, H.M.; Said, Z.; Raza, A.; Muyeen, S.M.; Nizami, A.-S.; Elavarasan, R.M.; Saidur, R.; Sopian, K. Energy storage technologies: An integrated survey of developments, global economical/environmental effects, optimal scheduling model, and sustainable adaption policies. *J. Energy Storage* **2023**, *72*, 108694, https://doi.org/10.1016/j.est.2023.108694.
3. Mousavi, S.M.; Hashemi, S.A.; Kalashgrani, M.Y.; Gholami, A.; Binazadeh, M.; Chiang, W.-H.; Rahman, M.M. Recent advances in energy storage with graphene oxide for supercapacitor technology. *Sustain. Energy Fuels* **2023**, *7*, 5176-5197, https://doi.org/10.1039/D3SE00867C.
4. Nowrot, A.; Manowska, A. Supercapacitors as Key Enablers of Decarbonization and Renewable Energy Expansion in Poland. *Sustainability* **2024**, *16*, 216, https://doi.org/10.3390/su16010216.
5. Yi, T.-F.; Sari, H.M.K.; Li, X.; Wang, F.; Zhu, Y.-R.; Hu, J.; Zhang, J.; Li, X. A review of niobium oxides based nanocomposites for lithium-ion batteries, sodium-ion batteries and supercapacitors. *Nano Energy* **2021**, *85*, 105955, https://doi.org/10.1016/j.nanoen.2021.105955.
6. Xia, R.; Zhao, K.; Kuo, L.-Y.; Zhang, L.; Cunha, D.M.; Wang, Y.; Huang, S.; Zheng, J.; Boukamp, B.; Kaghazchi, P.; Sun, C.; ten Elshof, J.E.; Huijben, M. Nickel Niobate Anodes for High Rate Lithium-Ion Batteries.*Adv. Energy Mater.* **2021**, *12*, 2102972, https://doi.org/10.1002/aenm.202102972.
7. Ansari, M.Z.; Ansari, S.A.; Kim, S.-H. Fundamentals and recent progress of Sn-based electrode materials for supercapacitors: A comprehensive review.*J. Energy Storage* **2022**, *53*, 105187, https://doi.org/10.1016/j.est.2022.105187.
8. Zhang, C.; Yang, Y.; Liu, X.; Mao, M.; Li, K.; Li, Q.; Zhang, G.; Wang, C. Mobile energy storage technologies for boosting carbon neutrality. *Innovation* **2023**, *4*, 100518, https://doi.org/10.1016%2Fj.xinn.2023.100518.
9. Geng, H.; Peng, Y.; Qu, L.; Zhang, H.; Wu, M. Structure Design and Composition Engineering of Carbon-Based Nanomaterials for Lithium Energy Storage. *Adv. Energy Mater.* **2020**, *10*, 1903030, https://doi.org/10.1002/aenm.201903030.
10. Liu, T.-R.; Chang, Y.-C.; Bayeh, A.W.; Wang, K.-C.; Chen, H.-Y.; Wang, Y.-M.; Chiang, T.-C.; Tang, M.-T.; Tseng, S.-C.; Huang, H.-C.; Wang, C.-H. Synergistic effects of niobium oxide–niobium carbide–reduced graphene oxide modified electrode for vanadium redox flow battery. *J. Power Sources* **2020**, *473*, 228590, https://doi.org/10.1016/j.jpowsour.2020.228590.
11. Akhter, R.; Maktedar, S.S. MXenes: A comprehensive review of synthesis, properties, and progress in supercapacitor applications. *J. Mater.***2023**, *9*, 1196-1241, https://doi.org/10.1016/j.jmat.2023.08.011.
12. Prabhakar Vattikuti, S.V.; Shim, J.; Rosaiah, P.; Mauger, A.; Julien, C.M. Recent Advances and Strategies in MXene-Based Electrodes for Supercapacitors: Applications, Challenges and Future Prospects.*Nanomaterials* **2024**, *14*, 62, https://doi.org/10.3390/nano14010062.
13. Worku, A.K.; Alemu, A.A.; Ayele, D.W.; Getie, M.Z.; Teshager, M.A. Recent advances in MXene-based materials for high-performance metal-air batteries. *Green Chem. Lett. Rev.* **2024**, *17*, 2325983, https://doi.org/10.1080/17518253.2024.2325983.

14. Ma, J.; Guo, X.; Xue, H.; Pan, K.; Liu, C.; Pang, H. Niobium/tantalum-based materials: Synthesis and applications in electrochemical energy storage. *Chem. Eng. J.* **2020**, *380*, 122428, https://doi.org/10.1016/j.cej.2019.122428.
15. Shi, H.; Sun, Z.; Lv, W.; Xiao, S.; Yang, H.; Shi, Y.; Chen, K.; Wang, S.; Zhang, B.; Yang, Q.-H.; Li, F. Efficient polysulfide blocker from conductive niobium nitride@graphene for Li-S batteries. *J. Energy Chem.* **2020**, *45*, 135-141, https://doi.org/10.1016/j.jechem.2019.10.018.
16. Pang, R.; Wang, Z.; Li, J.; Chen, K. Polymorphs of Nb_2O_5 Compound and Their Electrical Energy Storage Applications. *Materials* **2023**,*16*, 6956, https://doi.org/10.3390/ma16216956.
17. Gupta, H.; Kumar, M.; Sarkar, D.; Menezes, P.W. Recent technological advances in designing electrodes and electrolytes for efficient zinc ion hybrid supercapacitors. *Energy Adv.* **2023**, *2*, 1263-1293, https://doi.org/10.1039/D3YA00259D.
18. Zhang, X.; Yao, J.; Zhu, L.; Wu, J.; Wei, D.; Wang, Q.; Chen, H.; Li, K.; Gao, Z.; Xu, C.; Feng, X. Experimental and simulation investigation of thermal runaway propagation in lithium-ion battery pack systems. *J. Energy Storage* **2024**, *77*, 109868, https://doi.org/10.1016/j.est.2023.109868.
19. Tran, M.-K.; Mevawalla, A.; Aziz, A.; Panchal, S.; Xie, Y.; Fowler, M. A Review of Lithium-Ion Battery Thermal Runaway Modeling and Diagnosis Approaches. *Processes* **2022**, *10*, 1192, https://doi.org/10.3390/pr10061192.
20. Chen, H.; Zhang, T.; Hua, Y.; Gao, Q.; Han, Z.; Xu, Y.; Yang, K.; Xu, X.; Liu, X.; Wang, S. Simulation and comparative study of the effect of the electrical connection between the battery electrodes on the battery thermal behavior. *J. Energy Storage* **2023**, *72*, 108409, https://doi.org/10.1016/j.est.2023.108409.
21. Habib, A.K.M.A.; Hasan, M.K.; Issa, G.F.; Singh, D.; Islam, S.; Ghazal, T.M. Lithium-Ion Battery Management System for Electric Vehicles: Constraints, Challenges, and Recommendations. *Batteries* **2023**, *9*, 152, https://doi.org/10.3390/batteries9030152.